Virologica Sinica 39 (2024) 645–654

Contents lists available at ScienceDirect

Virologica Sinica

journal homepage: www.keaipublishing.com/en/journals/virologica-sinica
www.virosin.org

Research Article

Design of antiviral AGO2-dependent short hairpin RNAs

Yuanyuan Bie [a,b,c], Jieling Zhang [a,b,d], Jiyao Chen [a,b], Yumin Zhang [a,b], Muhan Huang [a,b], Leike Zhang [a,b,c], Xi Zhou [a,b,c,d,*], Yang Qiu [a,b,c,d,*]

[a] Key Laboratory of Virology and Biosafety, Wuhan Institute of Virology, Chinese Academy of Sciences, Wuhan 430071, China
[b] State Key Laboratory of Virology, Wuhan Institute of Virology, Chinese Academy of Sciences, Wuhan 430071, China
[c] University of Chinese Academy of Sciences, Beijing 100049, China
[d] School of Life Sciences, Division of Life Sciences and Medicine, University of Science and Technology of China, Hefei 230027, China

ARTICLE INFO

Keywords:
AgshRNA
Antiviral strategy
Machine learning model

ABSTRACT

The increasing emergence and re-emergence of RNA virus outbreaks underlines the urgent need to develop effective antivirals. RNA interference (RNAi) is a sequence-specific gene silencing mechanism that is triggered by small interfering RNAs (siRNAs) or short hairpin RNAs (shRNAs), which exhibits significant promise for antiviral therapy. AGO2-dependent shRNA (agshRNA) generates a single-stranded guide RNA and presents significant advantages over traditional siRNA and shRNA. In this study, we applied a logistic regression algorithm to a previously published chemically siRNA efficacy dataset and built a machine learning-based model with high predictive power. Using this model, we designed siRNA sequences targeting diverse RNA viruses, including human enterovirus A71 (EV71), Zika virus (ZIKV), dengue virus 2 (DENV2), mouse hepatitis virus (MHV) and severe acute respiratory syndrome coronavirus 2 (SARS-CoV-2), and transformed them into agshRNAs. We validated the performance of our agshRNA design by evaluating antiviral efficacies of agshRNAs in cells infected with different viruses. Using the agshRNA targeting EV71 as an example, we showed that the anti-EV71 effect of agshRNA was more potent compared with the corresponding siRNA and shRNA. Moreover, the antiviral effect of agshRNA is dependent on AGO2-processed guide RNA, which can load into the RNA-induced silencing complex (RISC). We also confirmed the antiviral effect of agshRNA *in vivo*. Together, this work develops a novel antiviral strategy that combines machine learning-based algorithm with agshRNA design to custom design antiviral agshRNAs with high efficiency.

1. Introduction

RNA interference (RNAi) is a conserved eukaryotic mechanism for post-transcriptional gene silencing, and is mediated by small non-coding RNAs, such as microRNAs (miRNAs) and small interfering RNAs (siRNAs). siRNAs are double-stranded (ds)RNAs with 2-nucleotide (nt) 3′ overhangs in the length of 19–24 nt, which are processed by host endoribonuclease Dicer from endogenous or exogenous long dsRNAs or short hairpin RNAs (shRNAs). miRNA are transcribed as primary miRNAs (pri-miRNAs) in the nucleus by RNA polymerase and are subsequently cleaved into ~70 nt pre-miRNAs by Drosha and DGCR8. The pre-miRNAs are then transferred to the cytoplasm and further processed by Dicer into mature miRNA duplexes. The siRNAs and miRNAs are integrated into Argonaute (AGO) proteins and form the RNA-induced silencing complex (RISC) (Ghildiyal and Zamore, 2009). Mammals possess four AGO proteins and only the AGO2 contains catalytic activity that cleaves the target RNA. siRNAs and miRNAs exhibit asymmetry with a preference for loading one strand (guide) RNA into RISC. The thermodynamic characteristics play a significant role in determining which strand of the duplex will be selected as the guide for incorporation into RISC (Ha and Kim, 2014). The other strand of the duplex (passenger) is subsequently cleaved and degraded. The mature RISC is composed of a single-stranded guide RNA that is annealed to a complementary target, directing degradation (complete complementary, siRNA) or translational (partial complementary, miRNA) repression (Bartel, 2018). Importantly, siRNAs or shRNAs can be delivered directly into the cell as chemically synthesized molecules and trigger the gene silencing, highlighting that RNAi is a powerful tool for gene knockdown and a promising therapeutic candidate. Besides, RNAi also functions as an intrinsic antiviral immunity in diverse eukaryotes (Schierhorn et al., 2022; Anobile and Poirier, 2023).

However, several risks obstructing RNAi applications still remain. A major concern is that few mismatches are tolerated by the RISC, which

* Corresponding authors.
E-mail addresses: yangqiu@wh.iov.cn (Y. Qiu), zhouxi@wh.iov.cn (X. Zhou).

https://doi.org/10.1016/j.virs.2024.05.001
Received 11 March 2024; Accepted 6 May 2024
Available online 9 May 2024

may lead to off-target effects via partial base pairing of siRNAs with mRNAs and the downregulation of unintended targets (Jackson et al., 2003; Birmingham et al., 2006; Wu and Belasco, 2008; Huntzinger and Izaurralde, 2011). In addition, the RISC-loaded passenger strand of siRNA may also knockdown other irrelevant genes (Hu et al., 2020). Furthermore, shRNAs may disrupt endogenous miRNA biogenesis by competing for protein factors (e.g., Dicer). Besides, high-level accumulation of siRNAs/shRNAs may lead to the activation of endogenous RNA sensors, such as Toll-like receptor 3 (TLR3) (Grimm et al., 2006, 2010). Based on these, designing highly efficient siRNAs/shRNAs is crucial for the success of RNAi-based therapies.

While Dicer processes the majority of miRNAs, some of them are Dicer-independent. Particularly, pre-miR-451, characterized by a short 17-nt stem and 4-nt loop, evades Dicer processing and is instead cleaved by AGO2, which cleaves the 3′arm of pre-miR-451 and produces only a 30-nt guide strand intermediate (Cheloufi et al., 2010; Cifuentes et al., 2010; Yang et al., 2010). The 3′ end of the intermediate is then processed by poly(A)-specific ribonuclease (PARN), generating the 23–26 nt mature miR-451 (Yoda et al., 2013). Multiple evidence have shown that AGO2-dependent shRNAs (agshRNAs), based on the structure of pre-miR-451, present significant advantages over traditional shRNAs and siRNA (Liu et al., 2013, 2015; Herrera-Carrillo et al., 2015, 2017a, 2019; Shang et al., 2015; Herrera-Carrillo and Berkhout, 2017; Gao et al., 2019; Alsing et al., 2022). The lack of a passenger-strand of agshRNA is anticipated to decrease the likelihood of off-target effects resulting from the RISC-loaded passenger strand. Moreover, agshRNAs are preferentially incorporated into AGO2, leaving the loading of endogenous miRNAs into other AGOs unaffected.

The treatment of viral infections continues to pose a significant challenge, due to the constant emergence of new-onset viruses and the variation among strains of known virus species. Since RNAi enables gene silencing of a selected target gene through complementary base pairing between siRNAs and the target mRNAs, it offers a promising approach for developing flexible antiviral therapies that can be rapidly applied to new viral sequences. For example, siRNAs targeted for different human viruses like respiratory syncytial virus (RSV), human immunodeficiency virus (HIV), hepatitis C virus (HCV), hepatitis B virus (HBV) and Ebola virus (EBOV) have been appearing in clinical trials (DeVincenzo et al., 2010; Davidson and McCray, 2011; Gish et al., 2011; Choi and Croyle, 2013; Gebert et al., 2014). So far, a large number of design and prediction algorithms for utilizing siRNAs or shRNAs to knockdown host genes are available (Huesken et al., 2005; Shabalina et al., 2006; Vert et al., 2006; Ichihara et al., 2007; Knott et al., 2014; Pelossof et al., 2017). However, very few bioinformatics resources have been developed regarding siRNAs targeting viruses. In this study, we utilized a logistic regression algorithm on a chemically siRNA efficacy dataset that had been previously published, and developed an algorithm that has a strong predictive capability. Moreover, we combined this machine learning-based siRNA prediction model with agshRNA design, developing a novel antiviral strategy to custom design antiviral agshRNAs. Using this strategy, we designed agshRNAs against a range of RNA viruses, including human enterovirus A71 (EV71), Zika virus (ZIKV), dengue virus 2 (DENV2), mouse hepatitis virus (MHV) and severe acute respiratory syndrome coronavirus 2 (SARS-CoV-2). Mechanistically, we identified that the antiviral effect of agshRNA is dependent on the production of single-stranded guide RNA processed by AGO2. We also evaluated the *in vivo* antiviral effect of agshRNA.

2. Material and methods

2.1. Machine learning model training

The siRNA features associated with high silencing efficiency that have been previously identified (Reynolds et al., 2004; Ichihara et al., 2007; Lisowiec-Wąchnicka et al., 2019) were summarized and combined as being the principle in this study to improve the representation of siRNA sequences (Table 1). The dataset containing 2431 siRNA sequences and the corresponding efficiency data were obtained from a publicly available dataset (Huesken et al., 2005). This dataset was randomly divided into training set (1999 siRNAs) and testing set (432 siRNAs). For each siRNA sequence, the passenger strand (sense strand for mRNA) was used to generate feature vector according to the principle mentioned above, and the feature matrix of total siRNA sequences was generated (Supplementary Table S1). The siRNAs with silencing efficiency higher than 0.7 were labeled as high, while others as low. We employed logistic regression to train the model with L2 regularization and the 'liblinear' solver. The parameters were further adjusted by five-fold cross-validation. The model was assessed by using the ROC curve and confusion matrix. Python library scikit-learn was used for this part.

2.2. Design of antiviral agshRNAs

Viral genome sequences were scanned using a 19-nt window to generate all potential siRNA sequences. These siRNA sequences were then aligned to human RefSeq database (download from NCBI) using Blast+ (v 2.12.0) with default strategy. siRNAs with a complete match at positions 3–7 in the nucleotide sequence and a total matching length more than 15 nt were considered to have off-target effects and were consequently excluded. The remaining sequences were evaluated using the machine learning-based model as noted above. Supplementary Table S2 summarizes all the siRNA sequences (passenger strand) targeting different viruses and the scores of sequences are ranked. To design agshRNA, the selected siRNA sequences were then extended from its 5′ end by two bases of viral genome sequences. The resulting 21-nt siRNA sequences were transformed to agshRNAs with 17-nt stem, 4-nt loop, and 2-nt U overhang at 3′ end according to the rule of agshRNA design (Herrera-Carrillo and Berkhout, 2017). A pipeline was generated to perform this process automatically. All the agshRNAs, shRNAs and siRNAs used in this study were synthesized by GenScript (Nanjing, China). The sequences of agshRNAs used here are listed in Supplementary Table S3.

2.3. Cell culture and transfection

HEK293T, rhabdomyosarcoma (RD), lung cancer A549, rat lung epithelial L2 and Vero E6 cells were maintained in Dulbecco's modified Eagle's medium (DMEM; Gibco, C11995500BT) supplemented with 10% FBS (Gibco, 10099-141C), 100 U/mL penicillin, and 100 μg/mL streptomycin at 37 °C in a humidified atmosphere with 5% CO_2. *A. albopictus* C6/36 cells were cultured in RPMI 1640 (Gibco, C11875500BT) medium containing 10% FBS at 27.5 °C. All cells mentioned above were commercially obtained from American Type Culture Collection (ATCC). The 293T NoDice cell line was kindly provided by B. R. Cullen (Durham, NC, USA) (Bogerd et al., 2014). The AGO2-KO 293T cell line was constructed via CRISPR/Cas9 system as previously described (Kong et al., 2023). Transfection was performed using Lipofectamine 2000 Reagent (Invitrogen, 11668019) according to the manufacturer's instructions.

Table 1
Principle of siRNA features.

Criterion	Feature value
I. 30%–52% G/C content	1/0
II. 'A/U' bases at positions 15–19	1/0 per position
III. Absence of internal repeats	1/0
IV. An "A" base at position 19 (sense strand)	1/0
V. An "A" base at position 3 (sense strand)	1/0
VI. An "U" base at position 10 (sense strand)	1/0
VII. A base other than "G" or "C" at 19 (sense strand)	1/0
VIII. A base other than "G" at position 13 (sense strand)	1/0
IX. Relative stability of the 5′ end of the siRNA duplex	1/0
X. The Gibbs free energy (ΔG) of siRNAs	normalized ΔG

2.4. Viruses and plaque assay

EV71 strain H (VR-1432) was amplified in RD cells (Fang et al., 2021). ZIKV strain GZ01 and DENV2 strain TSV01 were amplified in C6/36 cells (Lyu et al., 2022). MHV strain A59 was amplified in L2 cells (Wang et al., 2021). SARS-CoV-2 strain 2019-nCoV-WIV04 was amplified in Vero E6 cells (Xie et al., 2021). For plaque assay, vero cells in 12-well plates were infected with a 10-fold serial dilution of viruses. The cells were cultured at 37 °C for 1 h for viral adsorption. The supernatant 1% low-melting-point agarose (Sigma-Aldrich) in 2% FBS DMEM. After incubation at 37 °C for 2–3 days, cells were fixed with 4% formaldehyde and stained with 0.5% crystal violet to visualize the plaques.

2.5. RNA extraction and quantitative RT-PCR (qRT-PCR)

Total RNAs were extracted using Total RNA kit (Foregene, RE-03113) according to the manufacturer's instructions. The cDNA was obtained using Hifair AdvanceFast 1st Strand cDNA Synthesis Kit (Yeason, 11141ES60). The qRT-PCR was performed with the primers specific for the viral genomes of EV71, ZIKV, MHV, DENV2 and SARS-CoV-2. The qRT-PCR was performed using Hieff qPCR SYBR Green Master Mix (Yeasen, 11202ES08). All the primers used in this study are listed in Supplementary Table S6.

2.6. Northern blotting

For northern blotting, total RNAs were extracted using Trizol reagent (Takara, 9109) according to the manufacturer's instructions. Briefly, 10 μg of total RNAs was resolved on 7 M urea-18% PAGE and transferred to a Hybond-A nylon membrane (GE Healthcare, RPN303B). The membrane was cross-linked using 1-ethyl-3-(3-dimethylaminopropyl) carbodiimide (EDC) (Sigma-Aldrich, E7750). The membrane was then hybridized with digoxin (DIG)-labeled probes at 40 °C overnight. After washing, the membrane was incubated with anti-DIG antibody conjugated with alkaline phosphatase and exposed to a luminescent image analyzer LAS4,000 (Fuji Film). The synthetic 21- and 25-nt RNAs were used as size markers. The small RNA markers and DIG-labeled oligo RNA probes targeting agshEV71-h1-5p, agshEV71-h1-3p, and U6 were synthesized by Takara. All the RNA probes used in this study are listed in Supplementary Table S6.

2.7. Western blotting

Cell were harvested in lysis buffer [20 mmol/L Tris-HCl (pH 7.4), 150 mmol/L NaCl, 1% NP-40, 0.25% deoxycholate, and a protease inhibitor cocktail (MCE, HY-K0010)]. Lysates were then subjected to 10% SDS-PAGE and Western blotting according to our standard procedures (Fang et al., 2021; Kong et al., 2023). The antibodies used are as follows: anti-FLAG (MBL, M185-7, 1:2000), anti-AGO2 (Abcam, EPR10410, 1:1000), and anti-Tubulin (Protein Tech Group, HRP-66031, 1:2000), HRP-conjugated Goat Anti-Mouse IgG (Jackson ImmunoResearch, 115-035-003, 1:5000).

2.8. RNA-immunoprecipitation (RNA-IP)

Cells were lysed in a lysis buffer [20 mmol/L Tris–HCl (pH 7.4), 200 mmol/L NaCl, 2.5 mmol/L $MgCl_2$, 0.5% Triton X-100, 0.5 U/mL RNase inhibitor (Promega, N2515) and a protease inhibitor cocktail (MCE, HY-K0010)] at 4 °C for 1 h. Lysates were centrifuged at 12,000×*g* for 10 min at 4 °C and the post-nuclear lysates were split into two equal fractions, followed by incubation with 1:100 anti-AGO2 antibody (Abcam, EPR10410) or anti-mouse IgG (CST, #5946S) together with protein-A/G agarose beads (Beyotime, P2055) at 4 °C for 12 h, respectively. The antibody-bound complexes were washed and RNAs or proteins were extracted from the complexes and subjected to further analyses.

2.9. Small RNA sequencing and data analysis

Libraries of small RNAs were constructed using TruSeq Small RNA Library Preparation Kits (Illumina) according to manufacturer's protocols, and then sequenced by Illumina HiSeq 2000 at Bioacme (Wuhan, China). Quality control and adapter trimming process were performed using Trim Galore (v0.6.4) with default parameters (Kong et al., 2023), and reads length between 17 and 70 were used for subsequent analyses. The sequenced reads were aligned to the human genome (GRCh38) by using Bowtie2 (v2.3.5.1). Reads that cannot be aligned to the human genome (GRCh38) were then aligned to agshRNAs. The sequences and lengths of reads aligned to agshRNA were then determined using an in-house script. Reads mapped to the genome were further categorized as miRNA, tRNA, snoRNA etc. by using htseq-count (v0.11.2). Annotation file was downloaded from DASHR 2.0 (https://dashr2.lisanwanglab.org/).

2.10. RNA-seq and data analysis

Libraries of total RNAs were constructed using MGIEasy RNA Library Preparation Kits (BGI) according to manufacturer's protocols, and then sequenced by MGISEQ2000 (BGI) at Wuhan Institute of Virology, CAS. Quality control and adapter trimming were performed using Trim Galore (v0.6.4) with default parameter. All reads were mapped to the human genome (GRCh38) using Hisat2 (v2.1.0) and then annotated using htseq-count (v0.11.2). Annotation file was downloaded from NCBI. Annotated reads numbers were transformed into count per million reads (CPM). Statistical significance was evaluated via using the unpaired *t*-test and adjusted using Bonferroni correction. Different expression genes (DEGs) were defined by $|\log2FC| > 1$ and $P.adj < 0.05$.

2.11. Mouse experiments

Four-week-old C57BL/6 mice were purchased from the Beijing Vital River Laboratory Animal Technology Co (Beijing, China). Mice were tail vein injected with LNP-agshMHV-h1 (n = 6) or LNP-CT (n = 6) at 2 mg/kg of body weight. After 24 h, mice were intraperitoneally (i.p.) infected with 1×10^6 PFU of MHV. The mortalities and weights of infected mice were monitored daily for 8 days. Survival curves were plotted and analyzed via log-rank analysis with Mantel Cox method. In addition, two groups of mice were administrated with the same methods as noted above except that these mice were euthanized at day 4 post infection (dpi), and the liver tissues were harvested for subsequent analysis. All mice were maintained in individually ventilated cages in an animal biosafety level 2 (ABSL-2) facility and received care in compliance with Institutional Animal Care and Use Committee of Wuhan Institute of Virology.

2.12. Quantification and statistical analysis

Statistical analyses were conducted via GraphPad Prism (8.3.0.). Data are means ± SEM, and statistical significance was evaluated via using the unpaired *t*-test. *P* value <0.05 was considered statistically significant.

3. Results

3.1. Prediction of siRNAs with a logistic regression algorithm

To develop an algorithm for siRNA efficacy prediction, we chose a set of features to represent siRNA sequences. Reynolds et al. characterized the features of high silencing siRNAs, including 30%–52% G/C content, at least 3 'A/U' bases at positions 15–19, absence of internal repeats, an "A" base at position 19 (sense strand), an "A" base at position 3 (sense strand), an "U" base at position 10 (sense strand), a base other than "G" or "C" at 19 (sense strand) and a base other than "G" at position 13 (sense strand) (Reynolds et al., 2004). Moreover, the differences in the stability

of the 5′ end of the siRNA duplex can influence the selection of the siRNA guide strand (Ichihara et al., 2007). In addition, the Gibbs free energy (ΔG) of siRNAs are also highly correlated with the silencing efficiency (Lisowiec-Wąchnicka et al., 2019). We combined these features as being the principle (Table 1) to improve the representation of siRNA sequences.

We used the 2431 tested siRNAs in the (Huesken et al., 2005) dataset for siRNA silencing efficiency modelling. These experimentally tested siRNAs were normalized to obtain true silencing efficiencies. The siRNAs with silencing efficiency higher than 0.7 were considered as high silencing efficiency RNAs and the others as low silencing efficiency RNAs. These siRNAs were randomly divided into two parts, the training set containing 1999 siRNAs and the testing set containing 432 siRNAs. A widely-used machine learning algorithm, logistic regression (Sommer and Gerlich, 2013) was used for model training (Fig. 1A). We extracted sequence features of siRNAs in the dataset according to the principle summarized in Table 1 and transformed them into a feature matrix (Supplementary Table S1), which were then trained by this logistic regression model with the parameters of being adjusted by five-fold cross-validation. As a result, the AUC value of this model was 0.817 (Fig. 1B). The confusion matrix also showed that our model has a high accuracy (Fig. 1B). These results indicate that this machine learning-based model built by us is capable of predicting the silencing efficiency of siRNAs.

We sought to apply this model to predict siRNAs targeting viruses. EV71 that belongs to the genus *Enterovirus* of the family *Picornaviridae* and is the major causative pathogen for hand-foot-and-mouth disease (HFMD) was used for the initial investigation. We identified viral sequences by systematically scanning the EV71 genome sequences to generate a comprehensive list of potential siRNA sequences (Fig. 1C). These sequences were then used to align with the host genome and remove all possible off-target siRNA sequences. The remaining sequences were evaluated and scored using the machine learning model and ranked according to high-to-low scores (Supplementary Table S2).

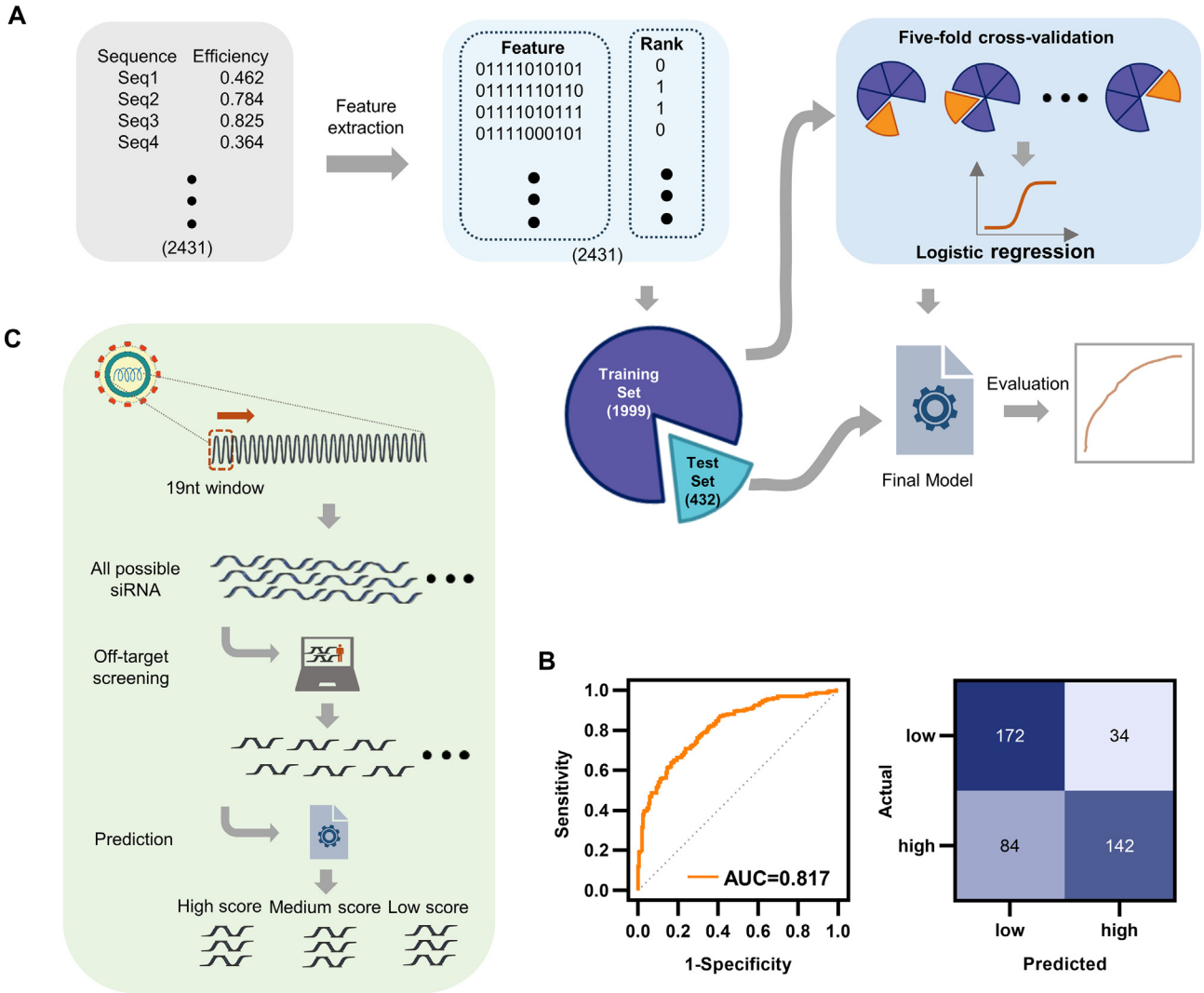

Fig. 1. Prediction of high efficiency antiviral siRNAs by using a machine-learning model. **A** Schematic for training the model to develop an efficacy predication algorithm. Set of siRNAs with known efficiency are collected from Huesken et al.'s work (Huesken et al., 2005). The siRNAs with silencing efficiency higher than 0.7 are considered as high efficiency (1) while others low efficiency (0). Dataset are randomly split into training set (1999 siRNAs) and testing set (432 siRNAs). The features of siRNAs in the dataset are extracted to build a feature matrix (Supplementary Table S1). Logistic regression was used to train the model and 5-fold cross-validation was performed to adjust model's parameter. Final model was tested using testing set. **B** Model performance evaluation using ROC curve (upper) and confusion matrix (lower). **C** Strategy to predict virus-targeting siRNAs with high efficiency. EV71 was used here as an example. Viral genome was scanned to generate all possible siRNAs, which were then aligned to host genome to remove potential off-target siRNAs. The remaining non-off-target siRNAs were evaluated using our model and the score of each sequence was ranked (Supplementary Table S2).

3.2. The antiviral strategy that combines machine learning-based siRNA prediction with agshRNA design

We sought to determine whether the predicted siRNAs could be developed into agshRNAs with potent antiviral activity. Thus, we selected the EV71-targeting siRNA sequence with the highest score in our model (Supplementary Table S2) as an example. This siRNA was named as siEV71-h1. The agshRNAs display the optimal AGO2-mediated processing activity with a stem length of 17/18-nt and a small loop of less than 5 nt (Herrera-Carrillo and Berkhout, 2017), while regular shRNAs processed by Dicer require a hairpin of at least 19 nt and a loop of more than 5 nt (Knott et al., 2014; Pelossof et al., 2017). The agshRNAs are more potent when U or A at the 5′-terminus and a short 3′-overhang of 1/3-nt (usually UU or UUU) at the 3′-terminus, the rule of which is also applied to shRNA design. Following it, we transformed siEV71-h1 to an agshRNA form (agshEV71-h1) with a 17-nt stem and a 4-nt loop (Fig. 2A, B). As a control, the shRNA form of siEV71-h1 (shEV71-h1) with a 22-nt stem and a 6-nt loop as well as the 3′ arm-located guide strand was also designed (Fig. 2B). It is noted that shRNAs with guide strands located in the 3′ arms of stems process strong silencing activity.

We examined the antiviral activities of these RNA molecules. RD cells were transfected with increasing concentrations of chemically synthesized agshEV71-h1, shEV71-h1 and siEV71-h1, respectively, and then infected with EV71 at a multiplicity of infection (MOI) of 0.1. At 24 hour post infection (hpi), the antiviral effects of different small RNA molecules were determined via measuring viral RNA accumulation with qRT-PCR. The siEV71-h1 displayed potent anti-EV71 activity in a dose-dependent manner with a 50% inhibitory concentration (IC_{50}) value of 0.37 nM (Fig. 2C), indicating that siEV71-h1 designed by our model has a high efficiency against EV71. Moreover, the shRNA form of siEV71-h1 (shEV71-1) showed more potent anti-EV71 activity ($IC_{50} = 0.14$ nmol/L, Fig. 2D) compared to that of siEV71-h1. Of note, the agshRNA form of siEV71-h1 (agshEV71-h1) exhibited the strongest antiviral activity with IC_{50} value of 0.011 nmol/L (Fig. 2E), showing that agshEV71-h1 presents significant advantages over siEV71-h1 and shEV71-h1. These results indicate that our siRNA prediction model can be combined with agshRNA design, leading to the development of agshRNAs with high antiviral efficiency.

We further evaluated the efficiency of this antiviral strategy that combines siRNA prediction model with agshRNA design. Thus, according to the siRNA sequences selected with different ranking scores (Supplementary Table S2), a series of agshEV71s (Supplementary Table S3) were designed and chemically synthesized. The agshEV71s contained siRNA sequences with top 3 highest, median 3 and lowest 3 scored were named as agshEV71-h1, -h2 and -h3, agshEV71-m1, -m2 and -m3, agshEV71-l1, -l2 and -l3, respectively. These agshEV71s were transfected into EV71-infected RD cells and the viral RNA accumulation was determined. We showed that anti-EV71 efficiencies of agshEV71s were consistent with the scoring results (Fig. 2F). Moreover, to investigate the potential off-target effects on endogenous genes, we performed RNA-sequencing using cells transfected with an equal amount of a control agshNC and agshEV71-h1. Transcriptomic analysis showed very few changes for the genes in the agshEV71-h1 group [agshEV71-h1 vs. agshNC $|\log2(FC)| > 1$, adjusted $P < 0.05$], including 4 up-regulation and 17 down-regulation genes (Supplementary Fig. S1 and Supplementary Table S4).

Furthermore, we applied this antiviral strategy into other viruses, including ZIKV and MHV. ZIKV belongs to mosquito-borne flavivirus responsible for neonatal microcephaly. MHV belongs to the coronavirus and can cause hepatitis in murine. The siRNA sequences targeting ZIKV and MHV with different ranking scores were predicted based on the machine learning-based algorithm, respectively (Supplementary Table S2). Subsequently, agshRNAs according to siRNA sequences with top 3 highest, median 3 and lowest 3 scores were designed and chemically synthesized (Supplementary Table S3). A549 and L2 cells were transfected with agshZIKVs and agshMHVs, and then infected with ZIKV and MHV at 0.1 MOI, respectively. The viral RNA accumulation was determined via qRT-PCR at 24 hpi. As shown in Fig. 2G, H, high-scoring agshZIKVs and agshMHVs exhibited potent antiviral activity against ZIKV and MHV, respectively. Moreover, antiviral efficiencies of agshZIKVs and agshMHVs displayed the consistent trend with the score ranking of siRNA sequences (Fig. 2G, H and Supplementary Table S2), similar to the data with agshEV71s.

In addition, we further designed agshRNAs targeting DENV2 and SARS-CoV-2 based on top 3 highest scored siRNA sequences (Supplementary Table S2) using the same strategy. DENV2 is a mosquito-borne flavivirus responsible for hemorrhagic fever, and SARS-CoV-2, belonging to coronavirus, cause the COVID-19 pandemic. A549 and Vero E6 cells were transfected with agshDENV2s and agshSARS-CoV-2s, and then infected with DENV2 and SARS-CoV-2 at 0.1 MOI, respectively. At 24 hpi, the viral RNA accumulation was determined via qRT-PCR. The agshDENV2s and agshSARS-CoV-2s also exhibited potent antiviral activities against ZIKV and MHV, respectively (Fig. 2I, J).

Together, our findings indicate that the antiviral strategy that combines machine learning-based siRNA prediction with agshRNA design can be effectively applied to different RNA viruses.

3.3. Antiviral effect of agshRNA is dependent on AGO2-processed guide RNA

We sought to determine whether agshRNAs confer antiviral activity via the RNAi pathway. Thus, normal 293T, Dicer-deficient 293T (NoDice) and AGO2-deficient (AGO2-KO) 293T cells were transfected with agshEV71-h1 and agshEV71-h2, respectively, and then infected with EV71 at an MOI of 0.1. We examined viral RNA replication at 24 hpi via qRT-PCR. The anti-EV71 activity of agshEV71-h1 or agshEV71-h2 was completely lost in AGO2-KO cells, but not affected in NoDice cells (Fig. 3A), showing the antiviral effect of agshRNAs are dependent on AGO2.

Moreover, we examined the production of agshEV71-derived guide RNA in normal, NoDice and AGO2-KO 293T cells by northern blotting via an RNA oligo probe complementary to the 5′arm (guide RNA) of agshEV71-h1 (agshEV71-5p). A RNA oligo probe targeting the 3′arm was used as the control (agshEV71-3p). As shown in Fig. 3B, the strand at the 5′arm but not at the 3′arm was detected in 293T cells, confirming that agshRNA only produces the single-stranded guide RNA. Furthermore, we found that AGO2 deficiency resulted in the complete absence of the guide RNA, while Dicer deficiency showed no effect on its production (Fig. 3B). These results are consistent with the findings that agshEV71s failed to inhibit EV71 replication in AGO2-KO cells (Fig. 3A), indicating that the antiviral effect of agshEV71s is dependent on AGO2-processed guide RNAs.

We noticed that the AGO2-processed guide RNA of agshEV71-h1 is ~25 nt in length with no trimmed form. For pre-miR-451, AGO2 cleaves the 3′arm and generates a 30-nt intermediate RNA, the 3′ end of which is then trimmed by PARN to generate ~23–26 nt mature miR-451 (Yoda et al., 2013). Thus, we examined whether the ~25-nt product of agshEV71-h1 can be trimmed by PARN. As a result, agshEV71-h1 cannot be further trimmed in cells overexpressing PARN (Fig. 3C). These results suggest that the antiviral activity of agshEV71-h1 is directed by the ~25-nt guide RNA, the length of which does not correspond to the normal mature miRNAs or siRNAs (~22-nt), which is consistent with the previous findings that the trimming is not an essential process for miRNA to function and the RISC can be functional with miRNAs longer than 22-nt (Yoda et al., 2013; Shang et al., 2015).

3.4. The guide RNAs derived from agshRNAs can effectively load into the RISC

To further examine the production of guide RNAs derived from agshRNAs, human 293T cells were transfected with agshEV71-h1, agMHV-h1 and agshZIKV-h1 for 24 h, and total RNAs were extracted and subjected to small RNA sequencing, respectively. As shown in

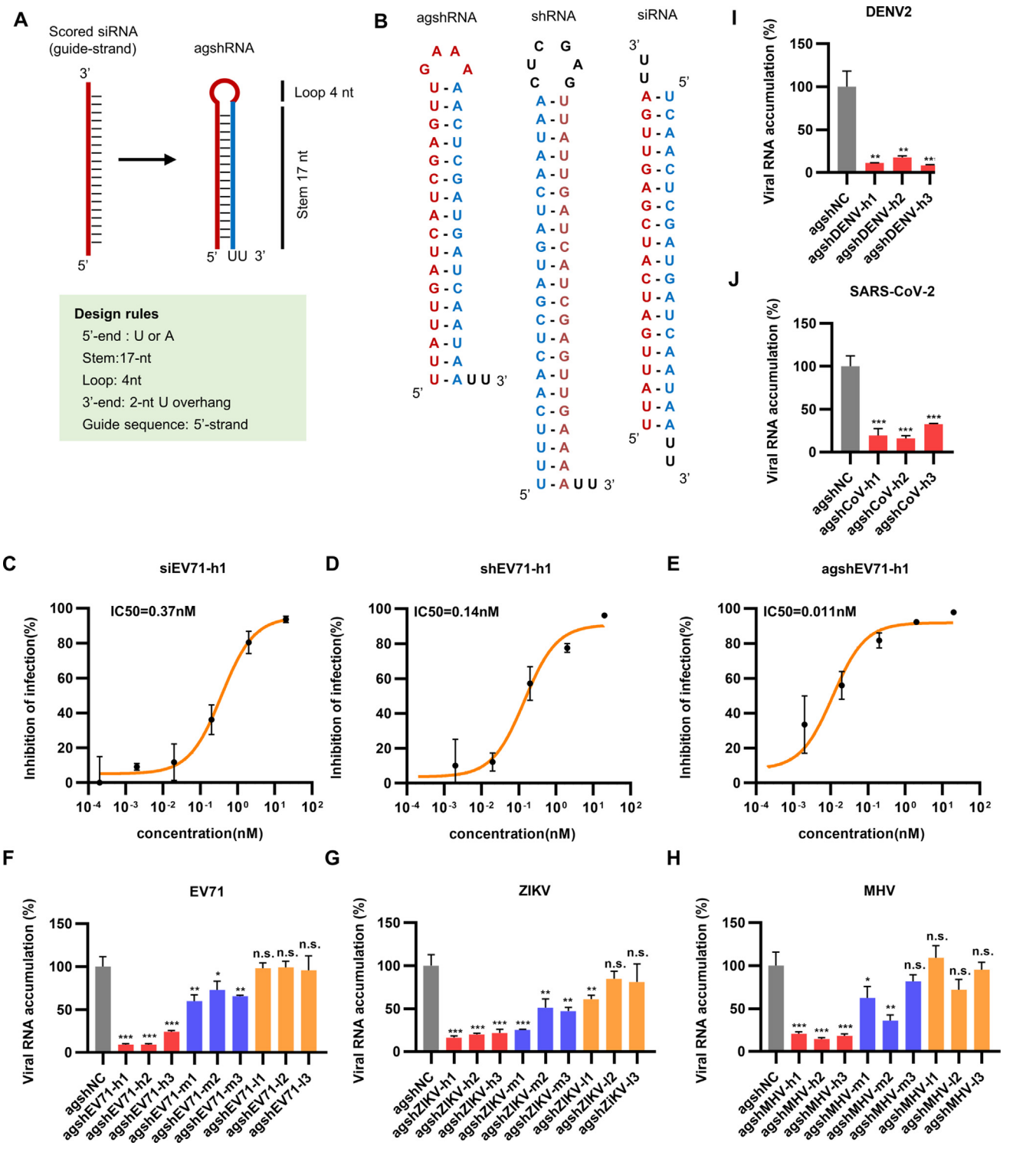

Fig. 2. The antiviral strategy that combines machine learning-based siRNA prediction with agshRNA design. **A** Schematic for transformation of siRNA sequences into agshRNA. **B** Design of agshEV71-h1, shEV71-h1, siEV71-h1 based on the same siRNA sequences with the highest score. Guide strands were shown in red and passenger strands in blue. **C–E** RD cells were transfected with siEV71-h1, shEV71-h1 and agshEV71-h1 with different concentrations indicated for 2 h, and then infected with EV71 (MOI = 0.1). At 24 hpi, total RNAs were extracted and subjected to qRT-PCR to detect the levels of EV71 genomic RNA. The IC_{50} value of each RNA molecule was determined. Data were means ± SEM from triplicate samples. **F–H** RD, A549 and L2 cells were transfected with the corresponding agshRNAs with top 3 highest, median 3 and lowest 3 scored siRNA sequences (agshEV71-h1, -h2 and -h3, agshEV71-m1, -m2 and -m3, agshEV71-l1, -l2 and -l3, 10 nmol/L for each) for 2 h, and then infected with EV71, ZIKV and MHV (MOI = 0.1 for each), respectively. AgshNC was used as the control in each group. At 24 hpi, total RNAs were extracted and subjected to qRT-PCR to detect the levels of viral genomic RNA, and the level of viral RNAs in cells with agshNC treatment was defined as 100%. Data were means ± SEM from triplicate samples. **I–J** A549 and Vero E6 cell were transfected with the corresponding agshRNAs with top 3 highest scored siRNA sequences (agshDENV2-h1, -h2 and -h3, agshSARS-CoV-2-h1, -h2 and -h3, 10 nmol/L for each) for 2 h, and then infected with DENV2 and SARS-CoV-2 (MOI = 0.1 for each), respectively. AgshNC was used as the control in each group. At 24 hpi, total RNAs were extracted and subjected to qRT-PCR to detect the levels of viral genomic RNA, and the level of viral RNAs in cells with agshNC treatment was defined as 100%. Data were means ± SEM from triplicate samples. $^{*}P < 0.1$; $^{**}P < 0.01$; $^{***}P < 0.001$; n.s., no significant.

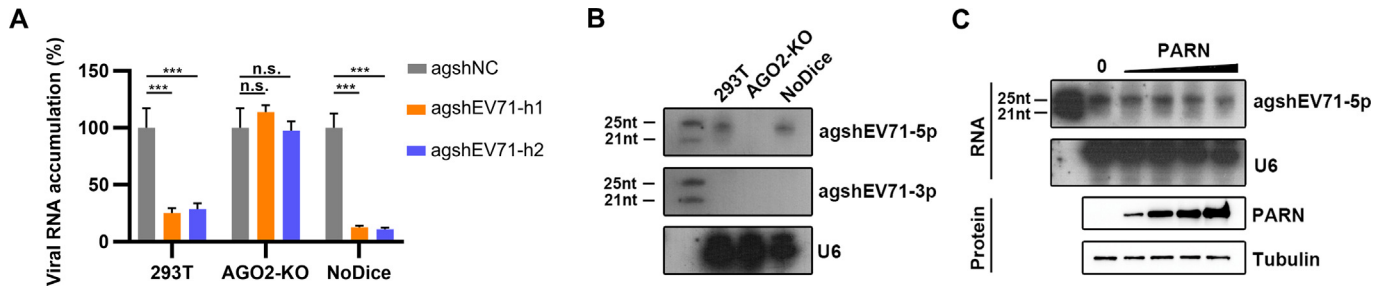

Fig. 3. Antiviral effect of agshRNA is dependent on AGO2-processed guide RNA. **A** Normal, NoDice and AGO2-KO 293T cell were transfected with agshEV71-h1, agshEV71-h2 and agshNC (10 nmol/L for each), respectively, and then infected with EV71 at an MOI of 0.1. At 24 hpi, total RNAs were extracted and subjected to qRT-PCR to detect the levels of EV71 genomic RNA, and the level of viral RNAs in infected cells with agshNC treatment was defined as 100%. Data were means ± SEM from triplicate samples.***$P < 0.001$; n.s., no significant. **B** Normal, NoDice and AGO2-KO 293T cell were transfected with agshEV71-1 (10 nmol/L). At 24 h post transfection, total RNAs were extracted and northern blot was performed to detect the 5′arm (5p) and the 3′arm (3p) of agshEV71-h1. The synthetic 21- and 25-nt RNAs were used as size markers. **C** 293T cell were transfected with increasing amounts of the plasmid encoding Flag-tagged PARN (0.18, 0.37, 0.75, 1.5 μg) together with agshEV71-h1 (10 nmol/L) for 24 h. Northern and western blottings were performed to detect the indicated RNAs and proteins, respectively.

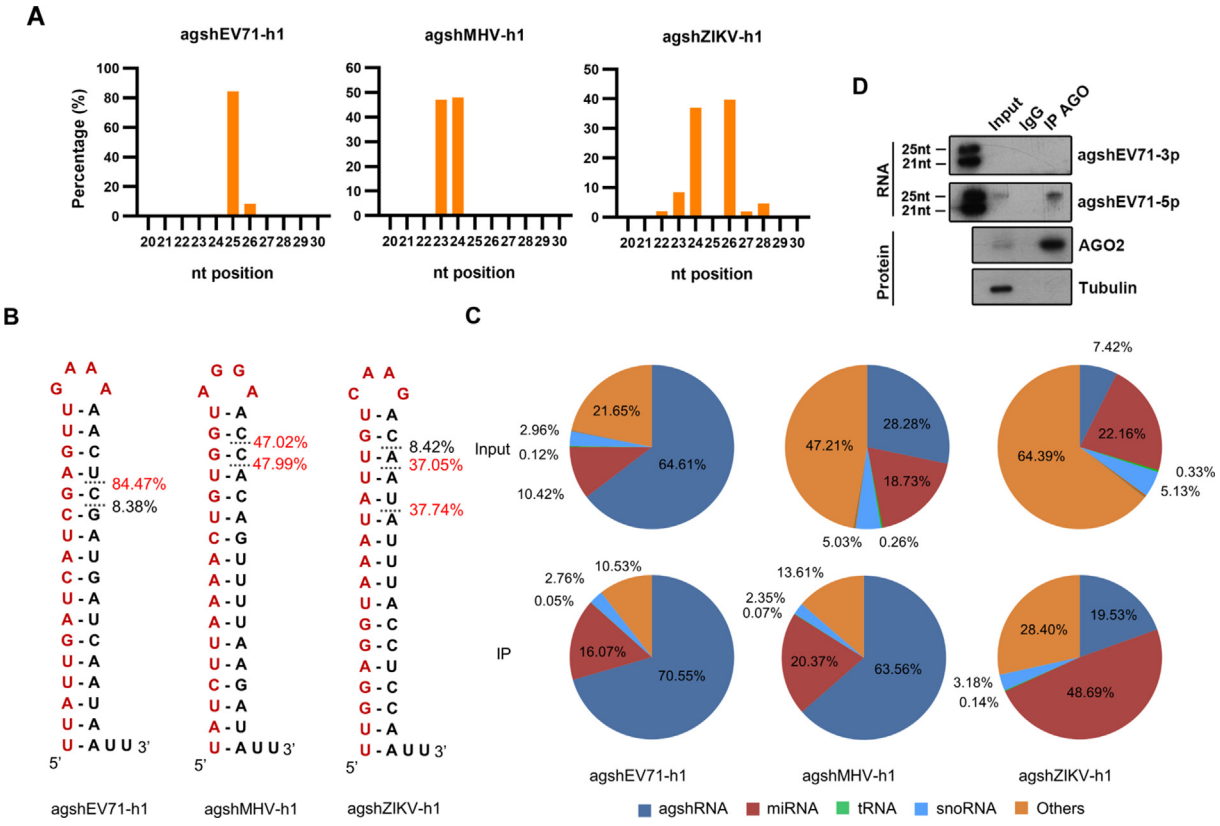

Fig. 4. The guide RNAs derived from agshRNAs load into the RISC. Human 293T cells were transfected with agshEV71-h1, agshMHV-h1, agshZIKV-h1 respectively (10 nmol/L for each). At 24 h post-transfection, cell lysates were subjected to RNA immunoprecipitation with an anti-AGO antibody or mouse IgG. Input and AGO-bound RNAs were prepared and subjected to deep sequencing. **A** The size distribution of agshRNAs-derived small RNAs in indicated input samples. **B** Processing of agshRNAs determined by deep-sequencing. Guide strands are shown in red. Dash lines show the 3′ end of guide strands, and the relative abundance is indicated next to the lines. **C** Relative abundance of endogenous small non-coding RNAs in input and IP samples. The relative abundances of small RNAs are shown in plat plot. This sequencing experiment was repeated twice independently, and the representative data was graphed (Supplementary Table S5, "agshEV71-h1#1-Input" and "agshEV71-h1#1-IP", "agshMHV-h1#1-Input" and "agshMHV-h1#1-IP", "agshZIKVh1#1-Input" and "agshZIKV-h1#1-IP"). **D** Northern and Western blottings were performed to detect input and precipitated small RNAs or proteins.

Fig. 4A, small RNA reads of AGO2-processed agshRNAs presented an overwhelming bias for the 5′arm strand (guide strand). For each agshRNA, the guide RNA possessed a homogenous 5′ end, while the 3′ end displayed some variation, resulting in guide strands of different lengths (Fig. 4B). Specifically, the vast majority (84.47% of total agshEV71-h1-derived small RNAs) of guide RNAs was 25-nt in length, consistent with the northern blotting results. In addition, agshMHV-h1 and agshZIKV-h1 produced two main guide RNAs with the lengths of 23-nt (47.02%) and 24-nt (47.99%), and 24-nt (37.05%) and 26-nt (37.05%), respectively, suggesting that these two agshRNAs underwent trimming.

To determine whether agshRNAs-derived RNA strands can load into the AGO-RISC, we sequenced small RNAs in the immunoprecipitates from agshRNAs-transfected cells by an anti-AGO antibody. We showed that agshRNAs-derived guide RNAs indeed loaded into AGO (Fig. 4C). Moreover, the abundance of AGO-bound guide RNAs were enriched in

RISCs compared with that of total guide RNAs without immunoprecipitation (Fig. 4C and Supplementary Table S5). Northern blot using agshEV71-h1 sample further confirmed the enrichment of guide RNAs into AGO (Fig. 4D). Together, our findings confirm that agshRNAs produce single-stranded guide RNAs that can load into the AGO-RISC.

3.5. AgshRNAs protect mice from lethal viral challenge

We sought to evaluate the antiviral effects of agshRNAs *in vivo*. MHV (strain A59) can cause lethal damage to liver after i.p. inoculation of 4–6-week-old C57BL/6 mice (Zhang et al., 2021). Thus, we utilized the MHV-infected mouse model to evaluate the antiviral effect of agshRNA. Lipid nanoparticles (LNPs) were used to prophylactically deliver agshMHV-h1. Four-week-old C57BL/6 mice were treated with LNP-agshMHV-h1 at a dose of 2 mg/kg or with LNP-agshNC via tail vein infection. After 24 h, mice were i.p. infected with 1×10^6 PFU of MHV, following monitored the mortalities and weights of infected mice for 8 days. The mice in the control group began to succumb to MHV infection from 6 dpi, and reached 66.7% mortality at 8 dpi. In contrast, 100% of the mice in the LNP-agshMHV-h1 group survived the viral challenge (Fig. 5A). Consistently, we observed significant differences of body weights between the LNP-agshMHV-h1 and control groups (Fig. 5B). In addition, the viral RNA accumulations of MHV in liver tissues were significantly reduced in the LNP-agshMHV-h1 group compared with those in the control group (Fig. 5C). Together, our findings showed that agshMHV-h1 had an effective *in vivo* antiviral effect on MHV infection.

4. Discussion

The utilization of RNAi-based therapeutics, such as siRNAs and shRNAs, exhibits significant promise for antiviral therapy. AGO2-dependent agshRNA displays significant advantages over traditional shRNA and siRNA (Herrera-Carrillo and Berkhout, 2017). In this study, we established an antiviral strategy that combines machine learning-based siRNA prediction and agshRNA design. Using this strategy, we developed a series of agshRNAs against a wide range of RNA viruses, including many important human pathogens. These agshRNAs displayed potent antiviral effects, which depended on the AGO2-processed single guide RNAs that can load into the RISC. The antiviral effect of agshRNA was also confirmed *in vivo*.

The design of siRNAs is challenging because a number of factors affect the efficacy of siRNAs, such as their GC content, nucleotides at siRNA termini, and thermodynamic properties. A number of siRNA prediction algorithms have been developed with the validated siRNAs. BIOPREDsi, a neural network approach, was trained on more than 2431 tested siRNAs and set as a fundamental performance standard (Huesken et al., 2005). Moreover, using the same dataset, many siRNA activity prediction algorithms based on machine learning models were built, including DSIR (Vert et al., 2006), ThermoComposition (Shabalina et al., 2006), and i-score (Ichihara et al., 2007). In addition, two algorithms, shERWOOD (Knott et al., 2014) and SplashRNA (Pelossof et al., 2017), were recently developed, which could predict shRNA that effectively and potently silence target genes. For siRNAs targeting viruses, however, very few bioinformatics resources have been developed. In this study, we established a machine learning-based algorithm based on the 2431 tested siRNAs, and combined this algorithm with agshRNA design to develop a novel antiviral strategy. Previous studies have suggested that siRNA design algorithms may not be applicable to the design of shRNA and most likely also agshRNA (Herrera-Carrillo et al., 2017b). Here we have shown that RNA viruses-targeting agshRNAs designed based on our strategy have potent antiviral efficiencies *in vitro* and *in vivo*. Moreover, this strategy improves the silencing efficiency of agshRNA to a level comparable or better than that of the corresponding shRNA and siRNA. Thus, the combination of machine learning-based siRNA prediction model and agshRNA design has the potential to achieve a promising antiviral strategy that can be effectively applied to different RNA viruses.

RNAi-based technology has innate advantages over small molecule therapeutics because siRNA executes its function by complete base pairing with mRNA, whereas small molecule drugs need to recognize the complicated spatial conformation of certain proteins. This feature confers the siRNA therapy with a shorter research and development span and a wider therapeutic area than small molecule drugs (Hu et al., 2020), which can quickly apply to any new RNA viruses. Moreover, the field of antiviral therapies utilizing gene editing such as CRISPR-Cas9 system is rapidly developing, but the application is also limited due to the low efficiency of targeted gene editing, off-target effects and safety (Marino et al., 2020).

The specific processing of agshRNA by AGO2 has several advantages over shRNA and siRNA. For shRNA or siRNA, the possibility of off-targeting effects is a major challenge, due to that a considerable portion of the passenger strand can still be incorporated into the RISC, even though the guide strand has thermodynamically less stable base pairing at its 5′ end a preference for loading into RISC (Jackson et al., 2003; Birmingham et al., 2006; Wu and Belasco, 2008; Huntzinger and Izaurralde, 2011). In terms of agshRNA, the single-stranded guide RNA cleavage by AGO2 completely eliminates the production of passenger strand (Liu et al., 2015). Moreover, AGO1/3/4 are unable to process agshRNA due to their lack of endonucleolytic activity. Thus,

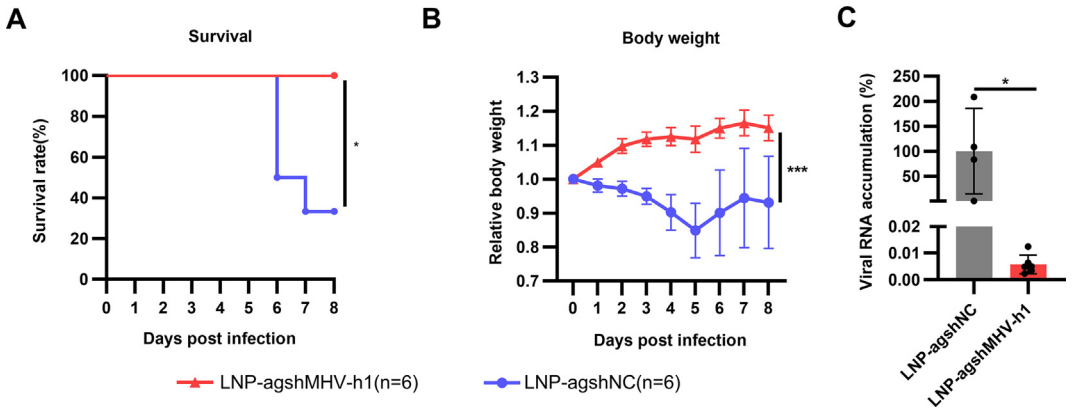

Fig. 5. AgshMHV protects mice from lethal MHV infection. **A** Four-week-old C57BL/6 female mice were tail vein injected with LNP-agshMHV-h1 (n = 6) or LNP-agshNC (n = 6) at 2 mg/kg of body weight. After 24 h, mice were challenged with 1×10^6 PFU of MHV-A59 via i.p. injection. Mouse survival was observed and recorded daily until 8 dpi. Statistical significance was evaluated via using Log-rank test. **B** Body weight changes of the different groups of mice in (**A**). **C** MHV-infected C57BL/6 mice treated with LNP-agshMHV-h1 or LNP-agshNC were detected via qRT-PCR. The level of MHV RNAs in LNP-agshNC-treated mice was defined as 100%. Two-way ANOVA was employed to analyze the overall differences in body weight change between the two groups of mice. $^*P < 0.1$; $^{***}P < 0.001$.

agshRNA-derived guide RNAs were exclusively associated with AGO2, reducing off-target effects (Shang et al., 2015). Our data showed that agshRNAs were processed by AGO2 into single-stranded guide RNAs. Consistent with this, antiviral effects of agshRNAs were found to be dependent on AGO2. Interestingly, agshRNAs produce guide RNAs of 23–26 nt in length, but no further trimmed shorter guide RNAs. These guide RNAs can effectively load into the RISC, although their lengths are higher than those of conventional mature miRNA. Our findings are consistent with previous observations that the 3′ trimming of miRNAs is not essential for target silencing and the RISC is functional with miRNAs longer than ~22 nt (Yoda et al., 2013; Shang et al., 2015).

Despite the promising prospects of agshRNA, its clinical application still needs to be investigated. The off-target effects of agshRNAs cannot be completely excluded because guide RNAs of agshRNAs within the RISC may also target unwanted genes via partial base pairing of guide RNAs with mRNAs. Besides, when intravenously injected, small RNAs including agshRNAs or siRNAs are rapidly cleared without being taken up by target cells due to the potent anionic charge of their phosphate backbone, which leads to electrostatic repulsion from the anionic surface of membranes (Wittrup and Lieberman, 2015). Multiple chemically modified geometries and delivery systems, such as nanoparticles and conjugates, have been developed to facilitate the small RNA delivery (Caillaud et al., 2020). Although these delivery systems still have certain limitations, including burst release, toxicity of cationic materials and fast uptake by mononuclear phagocyte system cells (Caillaud et al., 2020), much progress has been achieved for RNA-based drugs in preventing infectious disease (Skowronski and De Serres, 2021). In this study, based on the LNP system, we successfully protected mice from lethal MHV challenge by using agshMHV, which highlights the potent delivery efficacy of LNP-agshRNAs. These results suggest that our agshRNA design strategy together with LNP systems has promising clinical application potential in treating viral infections.

5. Conclusion

In summary, this work develops an antiviral strategy that combines machine learning-based siRNA prediction model with agshRNA design. Our findings provide a novel approach to custom design antiviral agshRNAs with high efficiency, which will shed light on the development of RNA drugs suitable for the emergence of any new RNA viruses.

Data availability

The sequencing data has been deposited to the ScienceDB (https://doi.org/10.57760/sciencedb.18146) and NCBI GEO database (GSE261262).

Ethics statement

All animal experiments were performed in strict accordance with the guidelines of the Chinese Regulations of Laboratory Animals (Ministry of Science and Technology of China) and approved by the Institutional Animal Care and Use Committee at Wuhan Institute of Virology, CAS.

Author contributions

Yuanyuan Bie: investigation, data curation, writing-original draft. Jieling Zhang: investigation, data curation, methodology. Jiyao Chen: investigation, formal analysis. Muhan Huang: investigation. Yumin Zhang: investigation. Leike Zhang: investigation. Xi Zhou: conceptualization, funding acquisition, writing-review&editing, supervision. Yang Qiu: conceptualization, funding acquisition, writing-review&editing, supervision.

Conflict of interest

Professor Xi Zhou is an editorial board member for *Virologica Sinica* and were not involved in the editorial review or the decision to publish this article. The authors declare that they have no conflict of interest.

Acknowledgements

We would like to thank the staff from Center for Instrumental Analysis and Metrology, Wuhan Institute of Virology, CAS for technical assistance. We thank all members of the Zhou lab for their support.

This work was supported by the National Key R&D Program of China (2023YFC2305900 to Y.Q. and X.Z.), the National Natural Science Foundation of China (U21A20423 to X.Z., 82172269 to Y.Q. and 82222028 to Y.Q.).

Appendix A. Supplementary data

Supplementary data to this article can be found online at https://doi.org/10.1016/j.virs.2024.05.001.

References

Alsing, S., Doktor, T.K., Askou, A.L., Jensen, E.G., Ahmadov, U., Kristensen, L.S., Andresen, B.S., Aagaard, L., Corydon, T.J., 2022. Vegfa-targeting mir-agshRNAs combine efficacy with specificity and safety for retinal gene therapy. Mol. Ther. Nucleic Acids 28, 58–76.

Anobile, D.P., Poirier, E.Z., 2023. RNA interference, an emerging component of antiviral immunity in mammals. Biochem. Soc. Trans. 51, 137–146.

Bartel, D.P., 2018. Metazoan micrornas. Cell 173, 20–51.

Birmingham, A., Anderson, E.M., Reynolds, A., Ilsley-Tyree, D., Leake, D., Fedorov, Y., Baskerville, S., Maksimova, E., Robinson, K., Karpilow, J., Marshall, W.S., Khvorova, A., 2006. 3' utr seed matches, but not overall identity, are associated with RNAi off-targets. Nat. Methods 3, 199–204.

Bogerd, H.P., Whisnant, A.W., Kennedy, E.M., Flores, O., Cullen, B.R., 2014. Derivation and characterization of dicer- and microRNA-deficient human cells. RNA 20, 923–937.

Caillaud, M., El Madani, M., Massaad-Massade, L., 2020. Small interfering RNA from the lab discovery to patients' recovery. J. Control. Release 321, 616–628.

Cheloufi, S., Dos Santos, C.O., Chong, M.M., Hannon, G.J., 2010. A dicer-independent miRNA biogenesis pathway that requires AGO catalysis. Nature 465, 584–589.

Choi, J.H., Croyle, M.A., 2013. Emerging targets and novel approaches to ebola virus prophylaxis and treatment. BioDrugs 27, 565–583.

Cifuentes, D., Xue, H., Taylor, D.W., Patnode, H., Mishima, Y., Cheloufi, S., Ma, E., Mane, S., Hannon, G.J., Lawson, N.D., Wolfe, S.A., Giraldez, A.J., 2010. A novel miRNA processing pathway independent of dicer requires argonaute2 catalytic activity. Science 328, 1694–1698.

Davidson, B.L., McCray Jr., P.B., 2011. Current prospects for RNA interference-based therapies. Nat. Rev. Genet. 12, 329–340.

DeVincenzo, J., Lambkin-Williams, R., Wilkinson, T., Cehelsky, J., Nochur, S., Walsh, E., Meyers, R., Gollob, J., Vaishnaw, A., 2010. A randomized, double-blind, placebo-controlled study of an RNAi-based therapy directed against respiratory syncytial virus. Proc. Natl. Acad. Sci. U. S. A. 107, 8800–8805.

Fang, Y., Liu, Z., Qiu, Y., Kong, J., Fu, Y., Liu, Y., Wang, C., Quan, J., Wang, Q., Xu, W., Yin, L., Cui, J., Xu, Y., Curry, S., Jiang, S., Lu, L., Zhou, X., 2021. Inhibition of viral suppressor of RNAi proteins by designer peptides protects from enteroviral infection in vivo. Immunity 54, 2231–2244.e2236.

Gao, Z., Berkhout, B., Herrera-Carrillo, E., 2019. Boosting agoshRNA activity by optimized 5'-terminal nucleotide selection. RNA Biol. 16, 890–898.

Gebert, L.F., Rebhan, M.A., Crivelli, S.E., Denzler, R., Stoffel, M., Hall, J., 2014. Miravirsen (spc3649) can inhibit the biogenesis of miR-122. Nucleic Acids Res. 42, 609–621.

Ghildiyal, M., Zamore, P.D., 2009. Small silencing RNAs: an expanding universe. Nat. Rev. Genet. 10, 94–108.

Gish, R.G., Satishchandran, C., Young, M., Pachuk, C., 2011. RNA interference and its potential applications to chronic HBV treatment: results of a phase i safety and tolerability study. Antivir. Ther. 16, 547–554.

Grimm, D., Wang, L., Lee, J.S., Schürmann, N., Gu, S., Börner, K., Storm, T.A., Kay, M.A., 2010. Argonaute proteins are key determinants of RNAi efficacy, toxicity, and persistence in the adult mouse liver. J. Clin. Invest. 120, 3106–3119.

Grimm, D., Streetz, K.L., Jopling, C.L., Storm, T.A., Pandey, K., Davis, C.R., Marion, P., Salazar, F., Kay, M.A., 2006. Fatality in mice due to oversaturation of cellular microRNA/short hairpin RNA pathways. Nature 441, 537–541.

Ha, M., Kim, V.N., 2014. Regulation of microRNA biogenesis. Nat. Rev. Mol. Cell Biol. 15, 509–524.

Herrera-Carrillo, E., Berkhout, B., 2017. Dicer-independent processing of small RNA duplexes: mechanistic insights and applications. Nucleic Acids Res. 45, 10369–10379.

Herrera-Carrillo, E., Harwig, A., Berkhout, B., 2015. Toward optimization of agoshRNA molecules that use a non-canonical RNAi pathway: variations in the top and bottom base pairs. RNA Biol. 12, 447–456.
Herrera-Carrillo, E., Harwig, A., Berkhout, B., 2017a. Silencing of HIV-1 by agoshRNA molecules. Gene Ther. 24, 453–461.
Herrera-Carrillo, E., Gao, Z., Berkhout, B., 2019. Influence of a 3' terminal ribozyme on agoshRNA biogenesis and activity. Mol. Ther. Nucleic Acids 16, 452–462.
Herrera-Carrillo, E., Gao, Z.L., Harwig, A., Heemskerk, M.T., Berkhout, B., 2017b. The influence of the 5′-terminal nucleotide on agoshRNA activity and biogenesis: importance of the polymerase iii transcription initiation site. Nucleic Acids Res. 45, 4036–4050.
Hu, B., Zhong, L., Weng, Y., Peng, L., Huang, Y., Zhao, Y., Liang, X.J., 2020. Therapeutic siRNA: state of the art. Signal Transduct. Target. Ther. 5, 101.
Huesken, D., Lange, J., Mickanin, C., Weiler, J., Asselbergs, F., Warner, J., Meloon, B., Engel, S., Rosenberg, A., Cohen, D., Labow, M., Reinhardt, M., Natt, F., Hall, J., 2005. Design of a genome-wide siRNA library using an artificial neural network. Nat. Biotechnol. 23, 995–1001.
Huntzinger, E., Izaurralde, E., 2011. Gene silencing by microRNAs: contributions of translational repression and mRNA decay. Nat. Rev. Genet. 12, 99–110.
Ichihara, M., Murakumo, Y., Masuda, A., Matsuura, T., Asai, N., Jijiwa, M., Ishida, M., Shinmi, J., Yatsuya, H., Qiao, S., Takahashi, M., Ohno, K., 2007. Thermodynamic instability of siRNA duplex is a prerequisite for dependable prediction of siRNA activities. Nucleic Acids Res. 35, e123.
Jackson, A.L., Bartz, S.R., Schelter, J., Kobayashi, S.V., Burchard, J., Mao, M., Li, B., Cavet, G., Linsley, P.S., 2003. Expression profiling reveals off-target gene regulation by RNAi. Nat. Biotechnol. 21, 635–637.
Knott, S.R.V., Maceli, A., Erard, N., Chang, K., Marran, K., Zhou, X., Gordon, A., Demerdash, O.E., Wagenblast, E., Kim, S., Fellmann, C., Hannon, G.J., 2014. A computational algorithm to predict shRNA potency. Mol. Cell 56, 796–807.
Kong, J., Bie, Y., Ji, W., Xu, J., Lyu, B., Xiong, X., Qiu, Y., Zhou, X., 2023. Alphavirus infection triggers antiviral RNAi immunity in mammals. Cell Rep. 42, 112441.
Lisowiec-Wąchnicka, J., Bartyś, N., Pasternak, A., 2019. A systematic study on the influence of thermodynamic asymmetry of 5'-ends of siRNA duplexes in relation to their silencing potency. Sci. Rep. 9, 2477.
Liu, Y.P., Schopman, N.C., Berkhout, B., 2013. Dicer-independent processing of short hairpin RNAs. Nucleic Acids Res. 41, 3723–3733.
Liu, Y.P., Karg, M., Harwig, A., Herrera-Carrillo, E., Jongejan, A., van Kampen, A., Berkhout, B., 2015. Mechanistic insights on the dicer-independent AGO2-mediated processing of AgoshRNAs. RNA Biol. 12, 92–100.
Lyu, B., Wang, C., Bie, Y., Kong, J., Wang, A., Jin, L., Qiu, Y., Zhou, X., 2022. Enoxacin shows broad-spectrum antiviral activity against diverse viruses by enhancing antiviral RNA interference in insects. J. Virol. 96, e0177821.
Marino, N.D., Pinilla-Redondo, R., Csörgő, B., Bondy-Denomy, J., 2020. Anti-CRISPR protein applications: natural brakes for CRISPR-Cas technologies. Nat. Methods 17, 471–479.
Pelossof, R., Fairchild, L., Huang, C.H., Widmer, C., Sreedharan, V.T., Sinha, N., Lai, D.Y., Guan, Y., Premsrirut, P.K., Tschaharganeh, D.F., Hoffmann, T., Thapar, V., Xiang, Q., Garippa, R.J., Rätsch, G., Zuber, J., Lowe, S.W., Leslie, C.S., Fellmann, C., 2017. Prediction of potent shRNAs with a sequential classification algorithm. Nat. Biotechnol. 35, 350–353.
Reynolds, A., Leake, D., Boese, Q., Scaringe, S., Marshall, W.S., Khvorova, A., 2004. Rational siRNA design for RNA interference. Nat. Biotechnol. 22, 326–330.
Schierhorn, K.L., Sanchez-David, R.Y., Maillard, P.V., 2022. Mammalian antiviral RNAi is on the move. EMBO J. 41, e111210.
Shabalina, S.A., Spiridonov, A.N., Ogurtsov, A.Y., 2006. Computational models with thermodynamic and composition features improve siRNA design. BMC Bioinformatics 7, 65.
Shang, R., Zhang, F., Xu, B., Xi, H., Zhang, X., Wang, W., Wu, L., 2015. Ribozyme-enhanced single-stranded AGO2-processed interfering RNA triggers efficient gene silencing with fewer off-target effects. Nat. Commun. 6, 8430.
Skowronski, D.M., De Serres, G., 2021. Safety and efficacy of the BNT162b2 mRNA COVID-19 vaccine. N. Engl. J. Med. 384, 1576–1577.
Sommer, C., Gerlich, D.W., 2013. Machine learning in cell biology - teaching computers to recognize phenotypes. J. Cell Sci. 126, 5529–5539.
Vert, J.P., Foveau, N., Lajaunie, C., Vandenbrouck, Y., 2006. An accurate and interpretable model for siRNA efficacy prediction. BMC Bioinformatics 7, 520.
Wang, C., Li, X., Ning, W., Gong, S., Yang, F., Fang, C., Gong, Y., Wu, D., Huang, M., Gou, Y., Fu, S., Ren, Y., Yang, R., Qiu, Y., Xue, Y., Xu, Y., Zhou, X., 2021. Multi-omic profiling of plasma reveals molecular alterations in children with COVID-19. Theranostics 11, 8008–8026.
Wittrup, A., Lieberman, J., 2015. Knocking down disease: a progress report on siRNA therapeutics. Nat. Rev. Genet. 16, 543–552.
Wu, L., Belasco, J.G., 2008. Let me count the ways: mechanisms of gene regulation by miRNAs and siRNAs. Mol. Cell 29, 1–7.
Xie, Y., Yin, W., Zhang, Y., Shang, W., Wang, Z., Luan, X., Tian, G., Aisa, H.A., Xu, Y., Xiao, G., Li, J., Jiang, H., Zhang, S., Zhang, L., Xu, H.E., Shen, J., 2021. Design and development of an oral remdesivir derivative VV116 against SARS-CoV-2. Cell Res. 31, 1212–1214.
Yang, J.S., Maurin, T., Robine, N., Rasmussen, K.D., Jeffrey, K.L., Chandwani, R., Papapetrou, E.P., Sadelain, M., O'Carroll, D., Lai, E.C., 2010. Conserved vertebrate miR-451 provides a platform for dicer-independent, AGO2-mediated microRNA biogenesis. Proc. Natl. Acad. Sci. U. S. A. 107, 15163–15168.
Yoda, M., Cifuentes, D., Izumi, N., Sakaguchi, Y., Suzuki, T., Giraldez, A.J., Tomari, Y., 2013. Poly(a)-specific ribonuclease mediates 3'-end trimming of argonaute2-cleaved precursor microRNAs. Cell Rep. 5, 715–726.
Zhang, Z., Liu, Q., Sun, Y., Li, J., Liu, J., Pan, R., Cao, L., Chen, X., Li, Y., Zhang, Y., Xu, K., Guo, D., Zhou, L., Lan, K., Chen, Y., 2021. Live attenuated coronavirus vaccines deficient in n7-methyltransferase activity induce both humoral and cellular immune responses in mice. Emerg. Microbes Infect. 10, 1626–1637.